Two-stage Transient-stability-constrained Optimal Power Flow for Preventive Control of Rotor Angle Stability and Voltage Sags

Jorge Uriel Sevilla-Romero, Alejandro Pizano-Martínez, Claudio Rubén Fuerte-Esquivel, and Reymundo Ramírez-Betancour

***Abstract*—In practice, an equilibrium point of the power system is considered transiently secure if it can withstand a specified contingency by maintaining transient evolution of rotor angles and voltage magnitudes within set bounds. A novel sequential approach is proposed to obtain transiently stable equilibrium points through the preventive control of transient stability and transient voltage sag (TVS) problems caused by a severe disturbance. The proposed approach conducts a sequence of non-heuristic optimal active power re-dispatch of the generators to steer the system toward a transiently secure operating point by sequentially solving the transient-stability-constrained optimal power flow (TSC-OPF) problems. In the proposed approach, there are two sequential projection stages, with the first stage ensuring the rotor angle stability and the second stage removing TVS in voltage magnitudes. In both projection stages, the projection operation corresponds to the TSC-OPF, with its formulation directly derived by adding only two steady-state variable-based transient constraints to the conventional OPF problem. The effectiveness of this approach is numerically demonstrated in terms of its accuracy and computational performance by using the Western System Coordinated Council (WSCC) 3-machine 9-bus system and an equivalent model of the Mexican 46-machine 190-bus system.**

***Index Terms*—Dynamic security assessment, transient stability, transient voltage sag (TVS), optimal power flow (OPF).**

NOMENCLATURE

A. Constants

$\delta_{\max}$	Limit of rotor angle
α	Rotor angle control (RAC) stage or transient voltage control (TVC) stage
λ	Percentage of magnitude of the maximum permissible active power re-dispatch in over-relaxed sequence of α ($O\text{-}SEQ_{\alpha}$)
$\boldsymbol{\tau}$	System parameters
Δt	Time step
η_{α}	Security criterion of α
η_{RAC}	Stability criterion of RAC
η_{TVC}	Admissible criterion of TVC
H_i	Inertia constant of the i^{th} generator
n_b	Number of buses
n_g	Number of generators
n_l	Number of loads
N_s	Number of integration steps Δt
P_{l_i}	Active power consumed by the i^{th} load l_i
t_{cl}	Fault clearing time
t_0^{+}	Disturbance inception time
t_{end}	End of experimental period
T	Study time period
$V_{\min}$	Limit of deep voltage

B. Functions

$\boldsymbol{f}(\cdot)$	Vector of differential functions
$f_E(\cdot)$	Cost function of generators
$\boldsymbol{g}(\cdot)$	Vector of algebraic functions
$\boldsymbol{G}(\cdot)$	Vector of power mismatch equations
$\boldsymbol{H}(\cdot)$	Vector of physical and operative limits of components
$P_{C\alpha}(\cdot)$	Projection of infeasible operating point in α
$P_C(\cdot)$	Projection operation

C. Sets and Operating Points

$\mathfrak{R}^{(\cdot)}$	Set of real numbers
$\boldsymbol{\Gamma}$	Set of time-invariant system parameters
$\boldsymbol{\theta}_{\beta}$	Set of voltage phase angles at OP_{β}
OP_{α}	Operating point where η_{α} is satisfied

Manuscript received: July 9, 2023; revised: October 14, 2023; accepted: December 2, 2023. Date of CrossCheck: December 2, 2023. Date of online publication: December 28, 2023.

This work was supported by the Fondo de Sustentabilidad Energética SENER-Conacyt, México (No. 246949, No. 249795).

J. U. Sevilla-Romero and C. R. Fuerte-Esquivel (corresponding author) are with the Faculty of Electrical Engineering, Universidad Michoacana de San Nicolás de Hidalgo, 58030 Morelia, México (e-mail: jorge.sevilla@umich.mx; claudio.fuerte@umich.mx).

A. Pizano-Martínez is with the Department of Electrical Engineering, University of Guanajuato, 36787 Salamanca, México (e-mail: apizano@ugto.mx).

R. Ramírez-Betancour is with the Department of Electrical and Electronic Engineering, Universidad Juárez Autónoma de Tabasco, 86040 Villahermosa, México (e-mail: reymundo.ramirez@ujat.mx).

DOI: 10.35833/MPCE.2023.000461

OP_β Operating point in $O\text{-}SEQ_\alpha$
OP_{h} Operating point in hull of $\boldsymbol{S}_\alpha$
OP_j Infeasible operating point of $P_{C\alpha}(\cdot)$
$OP_{in,\alpha}$ First stable operating point in $O\text{-}SEQ_\alpha$
OP_s Last unstable operating point in $O\text{-}SEQ_\alpha$
OP_{U} Transiently unstable operating point
OP_γ Operating point in under-relaxed sequence of α ($U\text{-}SEQ_\alpha$)
$\boldsymbol{P}_{g,\beta}$ Vector of active power of generators at OP_β
S_{F} Set of active power output of generators
S_α Subset of S_{F} where η_α is satisfied
S_{TVC} Subset of transient stability region in TVC stage
S_{RAC} Subset of transient stability region in RAC stage
$\boldsymbol{U}$ Vector of control variables
$\boldsymbol{V}_\beta$ Vector of voltage magnitudes at OP_β
$\boldsymbol{X}$ Vector of dynamic state variables
$\boldsymbol{Y}$ Vector of algebraic state variables

D. Variables

$\boldsymbol{\delta}(t)$ Dynamics vector of rotor angles at time t
$\delta_i(t)$ Rotor angle of the i^{th} generator at time t
$\delta_{COI}(t)$ Rotor angle of center of inertia δ_{COI} at time t
$\varphi^\alpha_{\beta t_u}$ Index in $O\text{-}SEQ_\alpha$
$\Delta\boldsymbol{P}^\alpha_{g,\gamma}$ Vector of active power re-dispatch in $U\text{-}SEQ_\alpha$
$\Delta\boldsymbol{P}^\alpha_{g,\beta}$ Vector of active power re-dispatch in $O\text{-}SEQ_\alpha$
$\Delta\boldsymbol{P}^\alpha_{g,\beta,\max}$ Vector of the maximum permissible active power re-dispatch in $O\text{-}SEQ_\alpha$
$\Delta\hat{\boldsymbol{P}}^\alpha_{g,\beta}$ Unit vector in direction of $\Delta\boldsymbol{P}^\alpha_{g,\beta}$
$\Delta\boldsymbol{P}^{Sch_\alpha}_{g,\beta}$ Vector of scheduled magnitude in $O\text{-}SEQ_\alpha$
$\Delta\hat{\boldsymbol{P}}^{Sch_\alpha}_{g,\beta}$ Vector of scheduled direction in $O\text{-}SEQ_\alpha$
$\Delta\boldsymbol{P}^{Sch_\alpha}_{g,\gamma}$ Vector of scheduled magnitude in $U\text{-}SEQ_\alpha$
$\Delta\hat{\boldsymbol{P}}^{Sch_\alpha}_{g,\gamma}$ Vector of scheduled direction in $U\text{-}SEQ_\alpha$
$\nabla_{\boldsymbol{P}_{g,\beta}}\varphi^\alpha_{\beta t_u}$ Gradient of $\varphi^\alpha_{\beta t_u}$ with regard to active power output of generators at current OP_β
j Number of current operating point for $O\text{-}SEQ_\alpha$
m Number of projections in $U\text{-}SEQ_\alpha$
$n_{\boldsymbol{x}}$ Number of dynamic state variables
$n_{\boldsymbol{y}}$ Number of algebraic state variables
$n_{\boldsymbol{u}}$ Number of control variables
$n_{\boldsymbol{\tau}}$ Number of time-invariant system parameters
P_{g_i} Active power production of the i^{th} generator
$P^{rO}_{C\alpha}(\cdot)$ Projection operation in $O\text{-}SEQ_\alpha$
$P^{rU}_{C\alpha}(\cdot)$ Projection operation in $U\text{-}SEQ_\alpha$
$P^{rO}_{C\alpha}(OP_\beta)$ Projection operation of OP_β in $O\text{-}SEQ_\alpha$
$P^{rU}_{C\alpha}(OP_\gamma)$ Projection operation of OP_γ in $U\text{-}SEQ_\alpha$
t_{u} Time to instability
T_γ Interval brackets OP_γ and $OP_{in,\alpha}$
Tol Convergence tolerance for $U\text{-}SEQ_\alpha$
$\boldsymbol{u}$ Vector of control variables
$V_k(t)$ Dynamics of voltage magnitudes $\boldsymbol{V}(t)$ at bus k
$\boldsymbol{V}(t)$ Nodal transient voltage magnitudes at time t
$\boldsymbol{x}(t)$ Dynamic state variables $\boldsymbol{x}$ at time t
$\boldsymbol{y}(t)$ Algebraic state variables $\boldsymbol{y}$ at time t

I. Introduction

THE occurrence of severe disturbances in power systems may lead to large excursions of rotor angles of the generator that cause transient instability and bus transient voltage sag (TVS) problems. The transient instability involves an irrevocable deviation among the transient trajectories of rotor angles of the generator that cause the loss of synchronism of generators. In contrast, TVS could trigger load shedding control actions as an emergency countermeasure against transient instability problems. Hence, the electric power system operating at a given equilibrium point can be declared insecure if the transient trajectories of rotor angles and bus voltage magnitudes are not bounded in response to a specific severe disturbance [1]. However, the transient evolution of trajectories can be bounded through effective control actions, which are preventively assessed and executed to lead the system to be a secure steady-state operating point. The active power re-dispatch of generators is one of the most effective control actions to ensure the security of power systems [1], [2]. Furthermore, this control action can be achieved in the most economical way by solving the transient-stability-constrained optimal power flow (TSC-OPF) problem [3], [4]. Based on the above consideration, this work focuses on determining an economically optimal equilibrium point that ensures the transient trajectories of rotor angles and voltage magnitudes are maintained within bounds when the electric power system is subjected to a severe disturbance.

Strictly speaking, the TSC-OPF problem is formulated as a semi-infinite optimal problem, where the objective is to minimize the active power re-dispatch cost subjected to equality and inequality constraints [5], [6]. The equality constraints represent the steady-state and dynamic operating state of the power system. In contrast, the set of inequality constraints keeps the transient trajectories of rotor angles and nodal voltage magnitudes within bounds [7]. The solution to this challenging problem focuses on deterministic- and evolutionary-based TSC-OPF approaches [3], [4], with the former being adopted in this work. The deterministic-based TSC-OPF approaches must transform the TSC-OPF model into a non-linear optimal problem that is solved by using existing non-linear programming methods [5], [6]. Depending on the transformation strategy adopted, different TSC-OPF approaches have been reported, with a comprehensive classification given in [3], [8], and [9]. These research works clearly show that only a few deterministic-based approaches, which are classified as simultaneous discretization (SD) [3], [7], and [10], multiple shooting (MS) [11], and single shooting (SS) [12] approaches, have considered the transient stability and TVS constraints for formulating the TSC-

OPF problem.

The SD approaches discretize the dynamic, transient stability, and TVS constraints at each time step associated with the numerical discretization of the stability study period. The entire set of constraints is directly included in the conventional optimal power flow (OPF) formulation, which results in a discrete non-linear TSC-OPF model that is solved as a single problem for control parameters, steady-state variables, and dynamic-state variables. Since the number of discretized constraints is proportional to the number of integration steps, the dimension of the TSC-OPF model is several orders higher than that of the traditional OPF model. Furthermore, since the set constraints must be simultaneously satisfied for every time step of the entire transient stability experimental period, the TSC-OPF problem suffers from enormous complexity and computational burden, so the solution may become intractable even for small-scale electric power systems [13].

MS [11] and SS [12] approaches simplify the solution of the TSC-OPF problem by replacing the dynamic constraints with time domain (TD) simulations, which are performed in each iteration of the optimization solution process to obtain the system dynamics. Based on the resulting system dynamics, the transient stability and TVS constraints are evaluated, and a sensitivity analysis is performed to numerically assess their corresponding gradients for solving the optimization problem. The MS approach has a moderate convergence rate and may impose an enormous computational burden because of the massive execution of TD simulations and sensitivity analysis [3]. In addition, the SS approach shows a slow convergence rate, and it fails in cases where the TD simulation and trajectory sensitivity analysis are ill-conditioned because of unbounded state trajectories [11].

An attractive strategy for solving the TSC-OPF problem is proposed by deterministic sequential approaches introduced in [13] and [14]. These approaches reformulate the TSC part as active power re-dispatch constraints. The TSC-OPF problem is then decomposed into two mutually connected subproblems: one associated with the OPF problem incorporating the active power re-dispatch constraints, and the other one with the transient stability assessment that obtains stability status of the transient trajectories of rotor angles, as well as the information required to assemble those re-dispatch constraints. Consequently, both subproblems are sequentially solved to force active power re-dispatches that gradually cancel out the rotor angle instability without including discretized constraints in the OPF problem. Therefore, the problem dimension, computational burden, and complexity are much lower than those in the SD, MS, and SS approaches. The drawback is that the formulation of the TSC part is based on heuristic criteria for active power re-dispatch, which may lead to suboptimal solutions [4]. Considering the suboptimal solution, the improved deterministic sequential approaches focused on the preventive control of the transient trajectories of rotor angles have been recently proposed, where the most economical active power re-dispatch is performed by considering a non-heuristic stability criterion during the preventive control process, e.g., in [15]-[21]. Even though the idea behind the deterministic sequential approaches is simple and intuitive, the approaches based on this concept have only focused on the preventive control of transient stability, e. g., without taking care of TVS in bus voltage magnitudes. The lack of control, however, for the transient evolution of voltage magnitudes within specified limits might activate load shedding schemes because of TVS. From the mathematical perspective, sequential approaches overlook TVS problems because the optimal problem is formulated solely in terms of steady-state variables. As a result, current sequential approaches cannot control TVS in voltage magnitudes. Thus, the proposed approach in this paper overcomes this problem, making such control possible by taking into account that, for large disturbances, TVS in voltage magnitudes is associated with significant excursions of generator rotor angles, as demonstrated in [1]. Consequently, the dynamics of voltage magnitudes can be controlled through active power re-dispatch.

Based on the preceding discussion, a deterministic non-heuristic sequential TSC-OPF approach is proposed, wherein both transient stability and TVS problems are seamlessly addressed. Therefore, the existence of two feasible operating regions is assumed: the transient stability region and admissible transient voltage sag (ATVS) region, which are composed of equilibrium points where the system subjected to a specified contingency scenario exhibits bounded evolutions of rotor angles and transient voltages. Furthermore, as directly inferred from the research works reported in [7], these two regions intersect in the parameter space of active power generation. Hence, to move the operating state of the system from a transiently infeasible operating point to an equilibrium point inside the intersection of both feasible operating regions, a sequence of non-heuristic active power re-dispatch is performed to initially steering the operating state of the system into the transient stability region and then into the ATVS region. These active power re-dispatches are performed by using the concept of projection of a point onto a set so that the proposed approach is composed of two projection stages: the rotor angle control (RAC) stage and the transient voltage control (TVC) stage [22], [23].

The approach reported in [19] has been adopted and reformulated to express the projection operation as an active power re-dispatch problem. The unique features and contributions of the proposed approach are the following.

1) The prevention of RAC stability and the TVS is performed by the proposed approach. The goal is achieved by introducing the concept of projection onto sets. The application of projections steers the operating state of the system towards an operating point where the transient trajectories of rotor angles and voltage magnitudes are bounded within pre-established limits.

2) The projection operation is formulated as a transiently constrained active power re-dispatch problem, so the projection corresponds to the solution of a slightly extended conventional OPF model, referred to as the TSC-OPF model, which has a dimension, complexity, and computational burden similar to that of a traditional OPF model.

3) The active power re-dispatch is generated non-heuristically by minimizing the transient excursions of rotor angles

and voltage magnitudes to the maximum rate of change with respect to the specified reference values. The non-heuristic active power re-dispatch also avoids the system overstabilization because the operating equilibrium point sought is projected in close proximity to the boundary of the ATVS region, as shown by the numerical results.

The rest of this paper is organized as follows. Section II provides the fundamentals of the proposed approach. Section III provides the formulation of the projection operation for performing the active power re-dispatch of generators. Section IV shows the proposed TSC-OPF approach, while case studies are presented in Section V. Lastly, Section VI reports the conclusions of this paper.

II. Fundamentals of Proposed Approach

The proposed approach consists of sequentially solving the transient stability and TSC-OPF problems until obtaining an equilibrium point that supports a specific disturbance, while maintaining the dynamics of rotor angles and transient voltage magnitudes is bounded within acceptable values according to their corresponding transient stability and TVS indices. This results in a dynamic system response, where the generators remain in synchronism without low transient voltage magnitudes, which causes the system to reach a secure steady-state equilibrium point.

In the proposed approach, the results obtained from the transient stability simulation when the system transient response is insecure because of the loss of transient stability or unbounded transient voltage magnitudes, provide the information needed to assemble the TSC-OPF model. This model is then solved to non-heuristically assess the optimal generation re-dispatch that steers the system to a transiently stable equilibrium point. In the sequential solution process, the equilibrium point obtained from the TSC-OPF model is provided as an initial operation condition for performing the transient simulation that allows determining if this equilibrium point is transiently stable.

A. Transient Stability and Trajectory Sensitivity Analysis

From the preventive security perspective, the power system at a given equilibrium point OP_β and subjected to a specified contingency scenario is declared transiently secure in terms of dynamics of rotor angles and voltage magnitudes if the following two criteria are simultaneously satisfied in a transient stability study [1]: η_{RAC} and η_{TVC}.

Stability criterion of RAC η_{RAC} states that the system synchronism is maintained when subjected to a severe disturbance if the transient trajectories of rotor angles do not surpass $\delta_{\max}$ with regard to $\delta_{COI}(t)$ during T, as given by (1) [12]. In this case, δ_{COI} is given by (2) [19].

$$\left|\delta_i(t)-\delta_{COI}(t)\right| \le \delta_{\max} \quad \forall t \in T, i=1,2,\ldots,n_g \tag{1}$$

$$\delta_{COI}(t)=\frac{\sum_{i=1}^{n_g} H_i \delta_i(t)}{H_T}=\frac{\sum_{i=1}^{n_g} H_i \delta_i(t)}{\sum_{i=1}^{n_g} H_i} \tag{2}$$

TVS in voltage magnitudes is associated with the rotor angle displacements occurring during a large disturbance [1]. Hence, to ensure a transiently secure response of the power system, the transient evolution of voltage magnitudes in all buses must be bounded within a pre-established limit [1]. In this paper, η_{TVC} states that voltage magnitudes $\boldsymbol{V}(t)$ are within secure bounds if their minimum values are greater than $V_{\min}$ during T [7], as given by (3).

$$V_k(t) > V_{\min} \quad \forall t \in T, k=1,2,\ldots,n_b \tag{3}$$

where $V_k(t)$ is the element of $\boldsymbol{V}(t)$.

To assess the transient response of the electric power system operating at OP_β, the transient trajectories and their sensitivities with regard to a control variable are obtained by combining a TD simulation and the staggered direct method (TD-SDM) [24]. TD-SDM analysis determines if OP_β satisfies (1) and (3) for a specified disturbance, and it also provides the information of evaluating the dynamic sensitivities of rotor angles and voltage magnitudes with regard to the active power of each generator, i.e., $\partial\delta_i(t)/\partial P_{g_i}$ and $\partial V_k(t)/\partial P_{g_i}$, respectively. These sensitivities are used to formulate the non-heuristic active power re-dispatch in the TSC-OPF model.

In TD simulation, the power system dynamics are formulated by the set of differential-algebraic equations (DAEs).

$$\begin{cases} \dfrac{\mathrm{d}\boldsymbol{x}(t)}{\mathrm{d}t}=\boldsymbol{f}(\boldsymbol{x}(t),\boldsymbol{y}(t),\boldsymbol{u},\boldsymbol{\tau}) \\ \boldsymbol{f}(\cdot)\colon \Re^{n_x+n_y+n_u+n_\tau} \rightarrow \Re^{n_x} \qquad \boldsymbol{x} \in \boldsymbol{X} \subset \Re^{n_x}, \boldsymbol{y} \in \boldsymbol{Y} \subset \Re^{n_y}, \boldsymbol{u} \in \boldsymbol{U} \subset \Re^{n_u} \\ \boldsymbol{0}=\boldsymbol{g}(\boldsymbol{x}(t),\boldsymbol{y}(t),\boldsymbol{u},\boldsymbol{\tau}) \\ \boldsymbol{g}(\cdot)\colon \Re^{n_x+n_y+n_u+n_\tau} \rightarrow \Re^{n_y} \qquad \boldsymbol{\tau} \in \boldsymbol{\Gamma} \subset \Re^{n_\tau} \end{cases} \tag{4}$$

In (4), the set of differential equations associated with the generators and their control units is denoted by the diffenertial functions $\boldsymbol{f}(\cdot)$, while the stator algebraic equations and power flow mismatch equations are represented by the functions $\boldsymbol{g}(\cdot)$.

The formulations of how sensitive the trajectories of state variables are with regard to the changes in the active power produced by the i^{th} generator are given by (5) [24]. The derivation of this set of equations is detailed in [25].

$$\begin{cases} \dfrac{\mathrm{d}\boldsymbol{x}_{P_{g_i}}}{\mathrm{d}t}=\dfrac{\partial \boldsymbol{f}(\cdot)}{\partial \boldsymbol{x}}\dfrac{\partial \boldsymbol{x}}{\partial P_{g_i}}+\dfrac{\partial \boldsymbol{f}(\cdot)}{\partial \boldsymbol{y}}\dfrac{\partial \boldsymbol{y}}{\partial P_{g_i}}+\dfrac{\partial \boldsymbol{f}(\cdot)}{\partial P_{g_i}} \\ \boldsymbol{x}_{P_{g_i}}(t_{\mathrm{cl}})=\boldsymbol{0} \\ \dfrac{\partial \boldsymbol{g}(\cdot)}{\partial \boldsymbol{x}}\dfrac{\partial \boldsymbol{x}}{\partial P_{g_i}}+\dfrac{\partial \boldsymbol{g}(\cdot)}{\partial \boldsymbol{y}}\dfrac{\partial \boldsymbol{y}}{\partial P_{g_i}}+\dfrac{\partial \boldsymbol{g}(\cdot)}{\partial P_{g_i}}=\boldsymbol{0} \\ \boldsymbol{g}_{P_{g_i}}(t_{\mathrm{cl}})=\boldsymbol{0} \end{cases} \quad i=1,2,\ldots,n_g \tag{5}$$

where $\boldsymbol{x}_{P_{g_i}}(\cdot)=\partial\boldsymbol{x}(\cdot)/\partial P_{g_i}$ and $\boldsymbol{y}_{P_{g_i}}(\cdot)=\partial\boldsymbol{y}(\cdot)/\partial P_{g_i}$ are the sensitivities of dynamic and algebraic states with regard to the changes of the active power output of the i^{th} generator, respectively; and $\mathrm{d}\boldsymbol{x}_{P_{g_i}}/\mathrm{d}t$ is a vector representing the dynamic evolution of sensitivities in time.

Under a given contingency scenario and a given equilibrium OP_β associated with either the RAC stage or TVC stage, the TD-SDM analysis conducts a step-by-step integration process, which solves (4) to obtain the time evolution of $\boldsymbol{x}(t)$ and $\boldsymbol{y}(t)$. The solution is performed during $T=[t_0^+, t_{\rm cl}]\bigcup(t_{\rm cl}, t_{\rm end}]$. At each time step $t\in(t_{\rm cl}, t_{\rm end}]$ of the integration process, the trajectory sensitivities are also calculated from (5), as detailed in [25], and $\eta_{\rm RAC}$ or $\eta_{\rm TVC}$ is checked as appropriate: (1) in the RAC stage or (3) in the TVC stage. If η_α is satisfied during T, the TD-SDM analysis ends at the time step $t=t_{\rm end}$, and OP_β is declared transiently stable. If not, OP_β is declared transiently unstable at the first time step $t\in(t_{\rm cl}, t_{\rm end}]$ in which η_α is not satisfied. In this case, the time step is considered as $t_{\rm u}$, and the TD-SDM analysis stops to avoid further integration time steps and reduce the computational burden. Under this unstable ending condition, the TD-SDM results below are used to perform the optimal active power re-dispatch through the TSC-OPF model.

1) In the RAC stage: ① $t=t_{\rm u}$; ② the values of the rotor angles of each $i^{\rm th}$ generator at $t_{\rm u}$, $\delta_i(t_{\rm u})\in\boldsymbol{x}$; and ③ the sensitivities $\partial\delta_i(t)/\partial P_{g_i}|_{t_{\rm u}}\in\boldsymbol{x}_{P_{g_i}}$, $i=1,2,\ldots,n_g$.

2) In the TVC stage: ① $t=t_{\rm u}$; ② the value of nodal voltage magnitudes at $t_{\rm u}$, $\boldsymbol{V}(t_{\rm u})\in\boldsymbol{y}$; and ③ the sensitivities $\partial V_k(t)/\partial P_{g_i}|_{t_{\rm u}}\in\boldsymbol{y}_{P_{g_i}}$, $k=1,2,\ldots,n_b$, $i=1,2,\ldots,n_g$.

B. Projection-based Optimal Power Re-dispatch

When the power system is operating at $OP_{\rm U}$ in a given contingency scenario, the preventive control performed by the proposed approach strives to assess a steady-state $OP_{\rm TVC}$, where $\eta_{\rm RAC}$ and $\eta_{\rm TVC}$ are simultaneously satisfied. Therefore, this approach considers the existence of two feasible subsets $S_{\rm RAC}$ and $S_{\rm TVC}$ composed of operating points in the parameter set $S_{\rm F}$, where criteria (1) and (3) are satisfied, respectively, when performing the TD-SDM analysis. Reference [7] shows that an operating point satisfying $\eta_{\rm TVC}$ also satisfies $\eta_{\rm RAC}$, which means that $S_{\rm TVC}$ associated with admissible TVS can be considered as a subset of $S_{\rm RAC}$: $S_{\rm TVC}\subseteq S_{\rm RAC}$. Hence, the operating point $OP_{\rm TVC}$ sought must lie in the intersection of $S_{\rm TVC}$ and $S_{\rm RAC}$: $OP_{\rm TVC}\in\{S_{\rm TVC}\bigcap S_{\rm RAC}\}$. The general approach of projecting $OP_{\rm U}$ onto $S_{\rm TVC}$ to obtain $OP_{\rm TVC}$ is explained below.

In a general context, the exact projection of OP_α onto a subset S_α assesses $OP_{\rm h}$ on the hull of $S_{\rm F}$ closest to OP_α [22]. This projection is performed at the maximum rate of change through a projection operation $P_C(\cdot)$, i.e., $P_C(\cdot)$: $OP_\alpha\rightarrow OP_{\rm h}$, by using the concepts of directional derivatives and gradients [22]. In the case of multiple sets, an alternating projection method that repeatedly executes exact projection operations is applied to obtain an operating point in the hull of the region defined by the intersection of multiple sets [22], [23]. Since $S_{\rm TVC}$ is a subset of $S_{\rm RAC}$ [7], the general alternating projection method is directly simplified as a two-stage projection method. A general description of the projection method is shown in Fig. 1. Without loss of generality, Fig. 1 shows this projection method based on the parameter space $S_{\rm F}$ of the active power output of two generators. The operating points $OP_{\rm U}$ and $OP_{\rm RAC}$ are projected onto $OP_{\rm RAC}$ and $OP_{\rm TVC}$, respectively, by performing an optimal re-dispatch of the active power of generators, which corresponds to $P_C(\cdot)$.

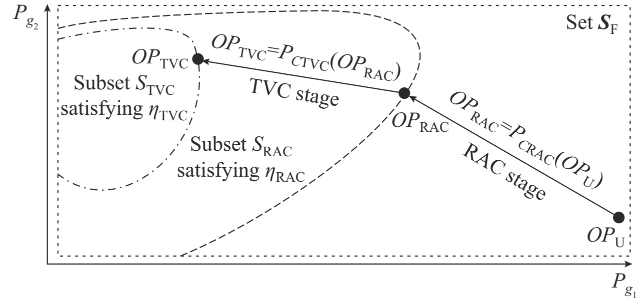

Fig. 1. General description of projection method.

As the stated above, the proposed approach is formulated in two general sequential projection stages: the RAC stage and TVC stage. The RAC stage first projects $OP_{\rm U}$ onto the hull of the subset $S_{\rm RAC}$ to obtain the $OP_{\rm RAC}$, where $\eta_{\rm RAC}$ is satisfied. $OP_{\rm RAC}$ is then projected onto the hull of the subset $S_{\rm TVC}$ in the TVC stage, which obtains the transiently stable $OP_{\rm TVC}$ sought. These two general stages are expressed in compact form by (6).

$$OP_\alpha=P_{C\alpha}(OP_j) \tag{6}$$

where $OP_j=OP_{\rm U}$ when $\alpha=$RAC, and $OP_j=OP_{\rm RAC}$ when $\alpha=$TVC.

The projection operation $P_{C\alpha}(\cdot)$ is formulated as a TSC-OPF problem based on a non-heuristic generation dispatch, as detailed in Section III.

III. Formulation of Projection Operators for Non-heuristic Generation Re-dispatch

In the α stage, the exact projection $P_{C\alpha}(\cdot)$ given by (6) cannot be directly performed since the subsets $S_{\rm RAC}$ and $S_{\rm TVC}$ are not known in advance. Hence, the general projection $P_{C\alpha}(\cdot)$ is achieved by executing the two correlated projection sequences, which are referred to as the over-relaxed sequence of α (*O-SEQ*$_\alpha$) and the under-relaxed sequence of α (*U-SEQ*$_\alpha$), respectively. The *O-SEQ*$_\alpha$ and *U-SEQ*$_\alpha$ sequences are shown in Fig. 2.

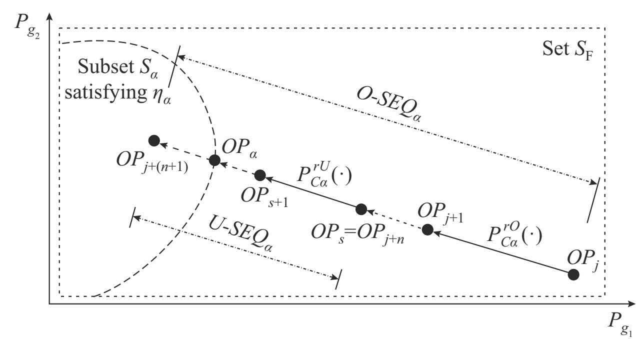

Fig. 2. *O-SEQ*$_\alpha$ and *U-SEQ*$_\alpha$.

The *O-SEQ*$_\alpha$ sequence recursively executes $P_{C\alpha}^{rO}(\cdot)$ to gradually displace the starting point OP_j until obtaining a first point $OP_{j+(n+1)}$ inside S_α, as denoted by (7), where η_α is satisfied.

$$OP_{\beta+1}=P_{C\alpha}^{rO}(OP_\beta)\quad \beta=j,j+1,\ldots,j+n \tag{7}$$

Since the operating point obtained in the $O\text{-}SEQ_\alpha$ sequence is not generally on the hall of S_α, which means that the system is over-stabilized, one must project this point onto that hall of S_α through the $U\text{-}SEQ_\alpha$ sequence. This goal is achieved by considering the last two operating points of the $O\text{-}SEQ_\alpha$ sequence that define an interval with the last unstable operating point and the first stable operating point, i.e., $OP_s = OP_{j+n}$ and $OP_{in,\alpha} = OP_{j+(n+1)}$, respectively, which bracket a critically stable OP_α on the hull of S_α. This interval is recurrently bisected by using projection operation $P_{C\alpha}^{rU}(\cdot)$ in the $U\text{-}SEQ_\alpha$ sequence, as indicated by (8), until obtaining a point $OP_{(s+m)+1}$ on the hull of S_α that corresponds to the sought OP_α, where η_α is satisfied.

$$OP_{\gamma+1} = P_{C\alpha}^{rU}(OP_\gamma) \quad \gamma = s, s+1, \dots, s+m \tag{8}$$

The projection operations $P_{C\alpha}^{rO}(\cdot)$ and $P_{C\alpha}^{rU}(\cdot)$ involved in (7) and (8), respectively, are formulated in the following subsections as an active power re-dispatch problem.

A. Projection Operation $P_{C\alpha}^{rO}(\cdot)$ in $O\text{-}SEQ_\alpha$ Sequence

When the $O\text{-}SEQ_\alpha$ sequence performed in the α stage, a new point $OP_{\beta+1}$ is obtained from a current point OP_β through $\Delta \boldsymbol{P}_{g,\beta}^\alpha \in \Re^{n_g}$, where $\Delta \boldsymbol{P}_{g,\beta}^\alpha$ represents the difference between the active power output of generators at OP_β and $OP_{\beta+1}$: $\Delta \boldsymbol{P}_{g,\beta}^\alpha = \boldsymbol{P}_{g,\beta+1}^\alpha - \boldsymbol{P}_{g,\beta}^\alpha$, $\boldsymbol{P}_{g,\beta}^\alpha$, $\boldsymbol{P}_{g,\beta+1}^\alpha \in \Re^{n_g}$. In the re-dispatch, some generators will decrease their active power output, and others will increase their generation level to satisfy the nodal balance of active power at the new point $OP_{\beta+1}$ [19].

The active power re-dispatch $\Delta \boldsymbol{P}_{g,\beta}^\alpha$, which corresponds to the projection operation $P_{C\alpha}^{rO}(\cdot)$, is represented by its magnitude $\Delta P_{g,\beta}^\alpha = \|\Delta \boldsymbol{P}_{g,\beta}^\alpha\|$ and a unit vector $\Delta \hat{\boldsymbol{P}}_{g,\beta}^\alpha$ in the direction of $\Delta \boldsymbol{P}_{g,\beta}^\alpha$, where $\Delta \hat{\boldsymbol{P}}_{g,\beta}^\alpha = \Delta \boldsymbol{P}_{g,\beta}^\alpha / \|\Delta \boldsymbol{P}_{g,\beta}^\alpha\|$ [19]. In this case, the magnitude $\Delta P_{g,\beta}^\alpha$ corresponds to the Euclidian norm or distance between OP_β and $OP_{\beta+1}$ in the parametric space of active power generation. Furthermore, the element values in the unit vector $\Delta \hat{\boldsymbol{P}}_{g,\beta}^\alpha$ indicate how that magnitude is distributed among the re-dispatchable generators to satisfy $\Delta \boldsymbol{P}_{g,\beta}^\alpha = \|\Delta \boldsymbol{P}_{g,\beta}^\alpha\| (\Delta \boldsymbol{P}_{g,\beta}^\alpha / \|\Delta \boldsymbol{P}_{g,\beta}^\alpha\|)$ [19]. The best active power re-dispatch corresponds to the one performed in the scheduled direction $\Delta \hat{\boldsymbol{P}}_{g,\beta}^\alpha$ and the scheduled magnitude $\Delta P_{g,\beta}^{Sch_\alpha}$, in which η_{RAC} and η_{TVC} are maximally improved. This theoretical condition is mathematically formulated by making the direction and magnitude of $\Delta \boldsymbol{P}_{g,\beta}^\alpha$ be $\Delta \hat{\boldsymbol{P}}_{g,\beta}^{Sch_\alpha}$ and $\Delta \boldsymbol{P}_{g,\beta}^{Sch_\alpha}$, respectively. These two references are derived, evaluated, and included in the TSC-OPF model as described below, which allows performing a projection operation $P_{C\alpha}^{rO}(\cdot)$. The projection operation in $O\text{-}SEQ_\alpha$ is shown in Fig. 3.

1) Formulation of Scheduled Direction $\Delta \hat{\boldsymbol{P}}_{g,\beta}^{Sch_\alpha}$

The criterion η_α is best improved through the active power re-dispatch when the formulation of the scheduled direction $\Delta \hat{\boldsymbol{P}}_{g,\beta}^{Sch_\alpha}$ is based on the gradient of the performance index $\varphi_{\beta t_\text{u}}^\alpha$ at t_u.

In the RAC stage, $\varphi_{\beta t_\text{u}}^\alpha$ is referred to as the transient stability index $\varphi_{\beta t_\text{u}}^{\text{RAC}}$.

Note that $\varphi_{\beta t_\text{u}}^{\text{RAC}}$ quantifies the level of coherence of the transient trajectories of rotor angles $\boldsymbol{\delta}(t) \in \Re^{n_g}$ at t_u, where η_{RAC} given by (1) is not satisfied.

$$\varphi_{\beta t_\text{u}}^{\text{RAC}} = \sum_{i=1}^{n_g} (\delta_i(t_\text{u}) - \delta_{COI}(t_\text{u}))^2 \tag{9}$$

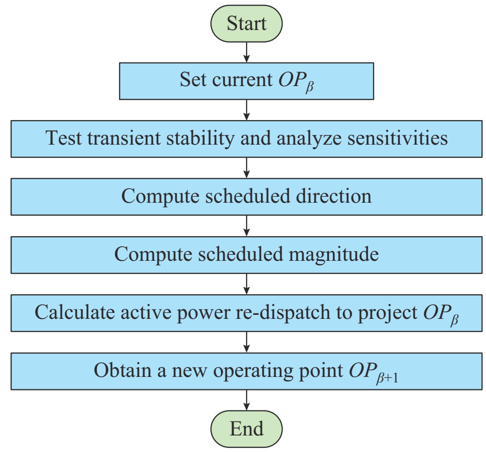

Fig. 3. Projection operation for $O\text{-}SEQ_\alpha$.

The performance index $\varphi_{\beta t_\text{u}}^\alpha$ given by (10) corresponds to the TVC stage. In this case, $\varphi_{\beta t_\text{u}}^{\text{TVC}}$ is referred to as the ATVS index and quantifies the deviation level for the trajectories of nodal transient voltages $\boldsymbol{V}(t) \in \Re^{n_b}$ at t_u with regard to a value of 1 p.u., where η_{TVC} given by (3) is not satisfied .

$$\varphi_{\beta t_\text{u}}^{\text{TVC}} = \sum_{i=1}^{n_b} (V_i(t_\text{u}) - 1)^2 \tag{10}$$

Based on the above, the most significant improvement in the transient evolution of the system is achieved when the active power re-dispatch at the current point OP_β is performed in the direction that reduces the value of performance index $\varphi_{\beta t_\text{u}}^\alpha$ at the maximum rate of change. Hence, the scheduled direction $\Delta \hat{\boldsymbol{P}}_{g,\beta}^{Sch_\alpha}$ is mathematically defined by the unitary vector given in [19].

$$\Delta \hat{\boldsymbol{P}}_{g,\beta}^{Sch_\alpha} = -\frac{\nabla_{\boldsymbol{P}_{g,\beta}} \varphi_{\beta t_\text{u}}^\alpha}{\|\nabla_{\boldsymbol{P}_{g,\beta}} \varphi_{\beta t_\text{u}}^\alpha\|} \tag{11}$$

Since $\varphi_{\beta t_\text{u}}^\alpha$ is not explicitly expressed in terms of the active power output of generators, as clearly shown in (9) and (10), $\nabla_{\boldsymbol{P}_{g,\beta}} \varphi_{\beta t_\text{u}}^\alpha$ is attained by using the chain rule given by (12), where the settings of elements $\varepsilon_k(t)$, $\varphi_{\beta t_\text{u}}^\alpha$, and u_b depend on the control stage that are being performed.

$$\nabla_{\boldsymbol{P}_{g,\beta}} \varphi_{\beta t_\text{u}}^\alpha = \left. \left(\frac{\partial \varphi_{\beta t_\text{u}}^\alpha}{\partial \varepsilon_k(t)} \frac{\partial \varepsilon_k(t)}{\partial P_{g_i}} \right) \right|_{t_\text{u}} \quad i = 1, 2, \dots, n_g \tag{12}$$

In the RAC stage, the settings are given by $\varepsilon_k(t) = \delta_k(t)$, $\varphi_{\beta t_\text{u}}^\alpha = \varphi_{\beta t_\text{u}}^{\text{RAC}}$, and $u_b = n_g$, which results in:

$$\nabla_{\boldsymbol{P}_{g,\beta}} \varphi_{\beta t_\text{u}}^{\text{RAC}} = \sum_{k=1}^{n_g} \left. \left(\frac{\partial \varphi_{\beta t_\text{u}}^{\text{RAC}}}{\partial \delta_k(t)} \frac{\partial \delta_k(t)}{\partial P_{g_i}} \right) \right|_{t_\text{u}} \quad i = 1, 2, \dots, n_g \tag{13}$$

In this case, the first partial derivative corresponds to (14), where $B = 1$ for $i = k$ and $B = 0$ for $\forall i \neq k$, and it is analytically obtained from (9).

$$\left.\frac{\partial \varphi_{\beta t_u}^{\text{RAC}}}{\partial \delta_i(t)}\right|_{t_u} = \sum_{i=1}^{n_g} 2(\delta_i(t_u) - \delta_{COI}(t_u))\left(B - \frac{H_i}{H_T}\right) \quad i = 1, 2, \ldots, n_g \tag{14}$$

The time evolution of rotor angles $\boldsymbol{\delta}(t)$ and their partial derivatives $\partial\delta_i(t)/\partial P_{g_i}$ involved in (14) and (13), respectively, are numerically obtained from the TD simulation and dynamic sensitivity analysis, as explained in Section II-A. In this case, the TD-SDM results used to evaluate (13) and (14) are as follows: ① t_u at which the criterion (1) is not satisfied; ② the values of rotor angles of the i^{th} generator at t_u $\delta_i(t_u) \in \boldsymbol{x}(t)$; and ③ the sensitivities $\partial\delta_i(t)/\partial P_{g_i}|_{t_u} \in \boldsymbol{x}_{P_{g_i}}$, $i = 1, 2, \ldots, n_g$.

Similarly, the gradient $\nabla_{\boldsymbol{P}_{g,\beta}} \varphi_{\beta t_u}^{\alpha}$ in the TVC stage is directly formulated by setting $\varepsilon_k(t) = V_k(t)$, $\varphi_{\beta t_u}^{\alpha} = \varphi_{\beta t_u}^{\text{TVC}}$, and $u_b = n_b$, which results in (15). The partial derivative $\partial\varphi_{\beta t_u}^{\text{TVC}}/\partial V_k(t)$ is given by (16), while the dynamics of nodal voltage magnitudes $\boldsymbol{V}(t) \in \Re^{n_b}$ and their sensitivities with regard to the active power generation are obtained from the TD-SDM analysis. Hence, the evaluation of (15) and (16) is based on the following TD-SDM results: ① t_u at which the criterion (3) is not satisfied; ② the value of nodal voltage magnitudes at t_u, $\boldsymbol{V}(t_u) \in \boldsymbol{y}$; and ③ the sensitivities $\partial V_k(t)/\partial P_{g_i}|_{t_u} \in \boldsymbol{y}_{P_{g_i}}$, $i = 1, 2, \ldots, n_g$, $k = 1, 2, ..., n_b$.

$$\nabla_{\boldsymbol{P}_{g,\beta}} \varphi_{\beta t_u}^{\text{TVC}} = \left.\sum_{k=1}^{n_b}\left(\frac{\partial \varphi_{\beta t_u}^{\text{TVC}}}{\partial V_k(t)} \frac{\partial V_k(t)}{\partial P_{g_i}}\right)\right|_{t_u} \quad i = 1, 2, \ldots, n_g \tag{15}$$

$$\left.\frac{\partial \varphi_{\beta t_u}^{\text{TVC}}}{\partial V_k(t)}\right|_{t_u} = 2\left(V_k(t_u) - 1\right) \quad k = 1, 2, \ldots, n_b \tag{16}$$

2) Formulation of Scheduled Magnitude $\Delta P_{g,\beta}^{Sch_\alpha}$

The value of $\Delta P_{g,\beta}^{Sch_\alpha}$ can be obtained from (17).

$$\Delta P_{g,\beta}^{Sch_\alpha} = \lambda \Delta P_{g,\beta,\max}^{\alpha} = \lambda \|\Delta \boldsymbol{P}_{g,\beta,\max}^{\alpha}\| \tag{17}$$

From a mathematical viewpoint, the active power re-dispatch $\Delta\boldsymbol{P}_{g,\beta,\max}^{\alpha}$ is obtained from the solution to the constrained optimial problem (18). In this model, the objective function maximizes the dot product representing the scalar projection of $\Delta\boldsymbol{P}_{g,\beta,\max}^{\alpha}$ onto the scheduled direction $\Delta\hat{\boldsymbol{P}}_{g,\beta}^{Sch_\alpha}$, subject to satisfying the lossless active power balance and the limits of active power generation. In this proposed formulation, $\Delta\boldsymbol{P}_{g,\beta,\max}^{\alpha} = \boldsymbol{P}_{g,\beta,\max}^{\alpha} - \boldsymbol{P}_{g,\beta}^{\alpha}$ such that the vector element $P_{g_i,\beta,\max}^{\alpha} \in \boldsymbol{P}_{g,\beta,\max}^{\alpha}$ is the active power output of the i^{th} generator with lower and upper active power limits $P_{g_i}^{\text{L}}$ and $P_{g_i}^{\text{U}}$, respectively.

$$\begin{cases} \min\limits_{\boldsymbol{P}_g} \boldsymbol{f}(\cdot) = -\Delta\boldsymbol{P}_{g,\beta,\max}^{\alpha} \cdot \Delta\hat{\boldsymbol{P}}_{g,\beta}^{Sch_\alpha} \\ \text{s.t.} \ \sum\limits_{i=1}^{n_g} P_{g_i,\beta,\max}^{\alpha} - \sum\limits_{i=1}^{n_l} P_{l_i} = 0 \\ \quad P_{g_i}^{\text{L}} \le P_{g_i,\beta,\max}^{\alpha} \le P_{g_i}^{\text{U}} \quad i = 1, 2, \ldots, n_g \end{cases} \tag{18}$$

Lastly, to avoid generators operating close to one of their limits and the computation of a transiently stable operating point far from the region boundary, which both can result from the projection operation $P_{C\alpha}^{rO}(\cdot)$, λ is set at a small value as 5%.

3) Formulation of $P_{C\alpha}^{rO}(\cdot)$ as TSC-OPF Problem

To project OP_β onto the feasible subset S_α, the conventional OPF model is slightly extended to force the re-dispatch $\Delta\boldsymbol{P}_{g,\beta}^{\alpha}$ to be performed with a magnitude $\Delta P_{g,\beta}^{Sch_\alpha}$ and direction $\Delta\hat{\boldsymbol{P}}_{g,\beta}^{Sch_\alpha}$ in the parametric space of generation. Hence, the resulting TSC-OPF model, which corresponds to the projection operation $P_{C\alpha}^{rO}(\cdot)$ described in (7), is given as follows.

$$\begin{cases} \min\limits_{\boldsymbol{P}_{g,\beta+1}, \boldsymbol{V}_{\beta+1}, \boldsymbol{\theta}_{\beta+1}} \boldsymbol{f}(\cdot) = \boldsymbol{f}_E(\boldsymbol{P}_{g,\beta+1}) - \dfrac{\Delta\boldsymbol{P}_{g,\beta}^{\alpha}}{\|\Delta\boldsymbol{P}_{g,\beta}^{\alpha}\|} \Delta\hat{\boldsymbol{P}}_{g,\beta}^{Sch_\alpha} \\ \text{s.t.} \ \boldsymbol{G}(\boldsymbol{V}_{\beta+1}, \boldsymbol{\theta}_{\beta+1}, \boldsymbol{P}_{g,\beta+1}) = \boldsymbol{0} \\ \quad \boldsymbol{H}(\boldsymbol{V}_{\beta+1}, \boldsymbol{\theta}_{\beta+1}, \boldsymbol{P}_{g,\beta+1}) \le \boldsymbol{0} \\ \quad \|\Delta\boldsymbol{P}_{g,\beta}^{\alpha}\|^2 - (\Delta P_{g,\beta}^{Sch_\alpha})^2 = 0 \end{cases} \tag{19}$$

where $\Delta\boldsymbol{P}_{g,\beta}^{\alpha} = \boldsymbol{P}_{g,\beta+1}^{\alpha} - \boldsymbol{P}_{g,\beta}^{\alpha}$.

Furthermore, the second term in the objective function forces the active power re-dispatch to be as close as possible to the scheduled direction $\Delta\hat{\boldsymbol{P}}_{g,\beta}^{Sch_\alpha}$, in which the system transient response is improved at the maximum rate of change. The last equality constraint assures that the Euclidian norm of the total amount of active power re-dispatched equals $\Delta P_{g,\beta}^{Sch_\alpha}$.

B. Projection Operation $P_{C\alpha}^{rU}(\cdot)$ in U-SEQ$_\alpha$

Once the point $OP_{in,\alpha} = OP_{j+(n+1)}$ inside S_α has been obtained, it is projected onto the hull of this feasible region through the projection operation $P_{C\alpha}^{rU}(\cdot)$. This projection is performed in *U-SEQ*$_\alpha$ of the α based on the point OP_γ and $OP_{in,\alpha}$ that bracket point OP_α on the hull of S_α: $T_\gamma = [OP_\gamma, OP_{in,\alpha}]$ such that $OP_\alpha \in T_\gamma$. Note that these operating points are known from the *O-SEQ*$_\alpha$ sequence. Moreover, the direction and magnitude of the active power re-dispatch that take the power system from the point OP_γ to $OP_{in,\alpha}$ are also known from (7) of the *O-SEQ*$_\alpha$ sequence, and they are denoted by $\Delta\hat{\boldsymbol{P}}_{g,\gamma}^{Sch_\alpha} = \Delta\hat{\boldsymbol{P}}_{g,j+n}^{Sch_\alpha}$ and $\Delta P_{g,\gamma}^{Sch_\alpha} = \Delta P_{g,j+n}^{Sch_\alpha}$, respectively.

Based on the information mentioned above, $P_{C\alpha}^{rU}(\cdot)$ determines the magnitude and the direction in which the active power re-dispatch must be performed from the current operating state OP_γ to obtain the new $OP_{\gamma+1}$. The flow chart of projection operation for *U-SEQ*$_\alpha$ is shown in Fig. 4.

The point $OP_{\gamma+1}$ is located in the middle of the interval T_γ, reducing the search interval for the subsequent execution of $P_{C\alpha}^{rU}(\cdot)$. Thus, similar to the projection operation $P_{C\alpha}^{rO}(\cdot)$ explained in Section III-A, the scheduled magnitude $\Delta P_{g,\gamma+1}^{Sch_\alpha}$, the scheduled direction $\Delta\hat{\boldsymbol{P}}_{g,\gamma+1}^{Sch_\alpha}$, and the formulation of the projection $P_{C\alpha}^{rU}(\cdot)$ in *U-SEQ*$_\alpha$ are described as below.

1) Formulation of Scheduled Magnitude $\Delta P_{g,\gamma+1}^{Sch_\alpha}$

The formulation and evaluation of the scheduled magnitude $\Delta P_{g,\gamma+1}^{Sch_\alpha}$ are achieved by halving the known magnitude $\Delta P_{g,\gamma}^{Sch_\alpha}$.

$$\Delta P_{g,\gamma+1}^{Sch_\alpha} = \frac{\Delta P_{g,\gamma}^{Sch_\alpha}}{2} \tag{20}$$

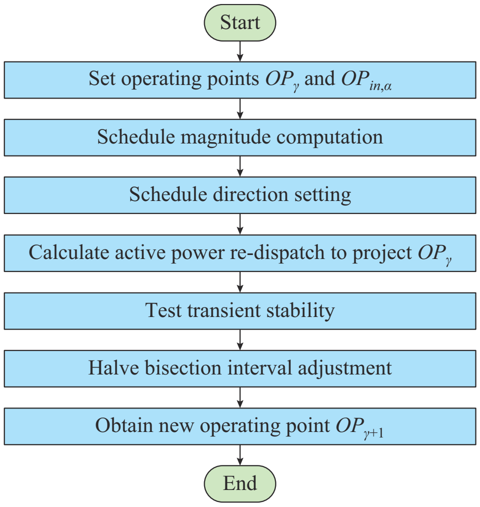

Fig. 4. Flow chart of projection operation in $U\text{-}SEQ_\alpha$.

2) Formulation of Scheduled Direction $\Delta\hat{\boldsymbol{P}}^{Sch_\alpha}_{g,\gamma+1}$

For $P^{rU}_{C\alpha}(\cdot)$, $\Delta\hat{\boldsymbol{P}}^{Sch_\alpha}_{g,\gamma+1}$ is fixed to the one that performs the last projection operation $P^{rO}_{C\alpha}(\cdot)$ in $U\text{-}SEQ_\alpha$: $\Delta\hat{\boldsymbol{P}}^{Sch_\alpha}_{g,\gamma+1}=\Delta\hat{\boldsymbol{P}}^{Sch_\alpha}_{g,\gamma}$.

3) Formulation of $P^{rU}_{C\alpha}(\cdot)$ as TSC-OPF Problem

Based on $\Delta P^{Sch_\alpha}_{g,\gamma+1}$ and $\Delta\hat{\boldsymbol{P}}^{Sch_\alpha}_{g,\gamma+1}$, the TSC-OPF model (19) is assembled and solved to obtain $OP_{\gamma+1}$. Thus, β in (19) must be replaced by γ, which results in (21), where $\Delta\boldsymbol{P}^{\alpha}_{g,\gamma}=\boldsymbol{P}^{\alpha}_{g,\gamma+1}-\boldsymbol{P}^{\alpha}_{g,\gamma}$.

$$\begin{cases}\min\limits_{\boldsymbol{P}_{g,\gamma+1},\boldsymbol{V}_{\gamma+1},\boldsymbol{\theta}_{\gamma+1}} \boldsymbol{f}(\cdot)=\boldsymbol{f}_E(\boldsymbol{P}_{g,\gamma+1})-\dfrac{\Delta\boldsymbol{P}^{\alpha}_{g,\gamma}}{\|\Delta\boldsymbol{P}^{\alpha}_{g,\gamma}\|}\Delta\hat{\boldsymbol{P}}^{Sch_\alpha}_{g,\gamma}\\ \text{s.t. } \boldsymbol{G}(\boldsymbol{V}_{\gamma+1},\boldsymbol{\theta}_{\gamma+1},\boldsymbol{P}_{g,\gamma+1})=\boldsymbol{0}\\ \quad\;\; \boldsymbol{H}(\boldsymbol{V}_{\gamma+1},\boldsymbol{\theta}_{\gamma+1},\boldsymbol{P}_{g,\gamma+1})\leq\boldsymbol{0}\\ \quad\;\; \|\Delta\boldsymbol{P}^{\alpha}_{g,\gamma}\|^2-(\Delta P^{Sch_\alpha}_{g,\gamma})^2=0\end{cases} \tag{21}$$

4) Adjustment of Interval $T_{\gamma+1}$

η_α is tested through the TD-SDM analysis applied to $OP_{\gamma+1}$. If η_α is not satisfied, OP_α is inside the interval $T_{\gamma+1}$ defined by $OP_{\gamma+1}$ and $OP_{in,\alpha}$ such that $T_{\gamma+1}=[OP_{\gamma+1},OP_{in,\alpha}]$. If η_α is satisfied, OP_α is inside the interval defined by the previous point OP_γ and the new point $OP_{\gamma+1}$. Hence, $T_{\gamma+1}=[OP_\gamma,OP_{\gamma+1}]$.

Lastly, the TD-SDM analysis is used to assess the transient evolution of the system at $OP_{\gamma+1}$, which does not require the sensitivity assessment for performing $P^{rU}_{C\alpha}(\cdot)$. This is because the scheduled direction remains fixed in $U\text{-}SEQ_\alpha$. Hence, the TD-SDM must only integrate the set of (4) to verify η_α and determine if $OP_{\gamma+1}$ is transiently stable.

C. Comparison with Other Models

The size and complexity comparison of TSC-OPF model is shown in Table I, which reveals the theoretical merits of the proposal and advances in reducing the size and complexity of the optimal problem regarding other models that perform system stability based on transient stability and TVS criteria. In this case, the conventional OPF problem is extended with only two constraints in the TSC-OPF problem, so both formulations have similar dimensions. Furthermore, the dimension of the TSC-OPF problem remains similar to the conventional OPF problem regardless of the size of the power system to be studied. In this paper, unlike the models reported in [7], [11], and [12], those two constraints do not depend on n_b, n_g, and N_s. Hence, the proposed approach avoids including the discrete-time equations of the multi-machine system in the OPF problem. The TD simulations required to compute the transient stability and TVS constraints are performed for a short study time period given by $T=[t_0^+,t_\text{u}]$: $t_\text{end}=t_\text{u}$. Note that these simulations are executed outside the TSC-OPF problem and only once at each iteration of the stabilization process. This is not the case for the proposals reported in [11] and [12], where the TD simulations must be executed at each iteration of the optimization process to obtain their corresponding transient stability and TVS constraints.

TABLE I
SIZE AND COMPLEXITY COMPARISON OF TSC-OPF MODEL

Model	t_end	N_s	Number of transient stability constraints*	Number of dynamic constraints	Number of TVS constraints	Heuristic stability criterion
SD [7]	Arbitrary	$N_s=(t_\text{end}-t_\text{cl}^+)/\Delta t$ arbitrary selected	N_s	$(2n_b+2n_g)N_s$	n_bN_s	No
SS [12]	Not required	0	1	0	n_b	No
MS [11]	Arbitrary	N_s arbitrary selected	n_gN_s	$(2n_b+2n_g)N_s$	n_bN_s	No
Proposed	Not required	0	2	0	2	No

Note：* means considering classical generator model.

IV. TSC-OPF APPROACH FOR PREVENTIVE CONTROL

The proposed approach is formulated by expressing the RAC and TVC stages in terms of $O\text{-}SEQ_\alpha$ and $U\text{-}SEQ_\alpha$ given by (7) and (8), respectively.

Considering $OP_j=OP_\text{U}$ as the starting point, (7) and (8) are performed once to achieve the RAC stage, which obtains the point $OP_\alpha=OP_\text{RAC}$. OP_RAC is then considered as the starting point OP_j in the TVC stage to obtain the point $OP_\alpha=OP_\text{TVC}$ through a new application of $O\text{-}SEQ_\alpha$ and $U\text{-}SEQ_\alpha$.

The step-by-step procedure of the proposed approach for solving the TSC-OPF problem is given as follows.

Step 1: for $\alpha=$RAC or $\alpha=$TVC, do the following.

Step 2: set the starting point OP_j in $O\text{-}SEQ_\alpha$ as $OP_j=OP_\text{U}$ when $\alpha=$RAC. Conversely, set $OP_j=OP_\text{RAC}$ when $\alpha=$TVC.

Step 3: perform $O\text{-}SEQ_\alpha$. In this case, the projection operation $OP_{\beta+1}=P^{rO}_{C\alpha}(OP_\beta)$ must be conducted for $\beta=j, j+1,\ldots, j+n$, describing as follows.

Step 3-1: execute the TD-SDM analysis for the specified contingency scenario to verify compliance with η_α for point OP_β. If η_α is satisfied, go to *Step 3-6*. Otherwise, the TD-SDM analysis provides the following results: ① the values of t_u; ② $\delta_k(t_u)$ and $\partial\delta_k(t)/\partial P_{g_i}|_{t_u}$, $k=1,2,\ldots,n_b$, $i=1,2,\ldots,n_g$ when $\alpha=$ RAC or $t=t_u$; and ③ $V_k(t_u)$ and $\partial V_k(t)/\partial P_{g_i}|_{t_u}$, $k=1, 2,\ldots,n_b$, $i=1,2,\ldots,n_g$ when $\alpha=$ TVC.

Step 3-2: evaluate the gradient $\nabla_{\boldsymbol{P}_{g,\beta}}\varphi^{\alpha}_{\beta t_u}$ from (13) when $\alpha=$ RAC or from (15) when $\alpha=$ TVC.

Step 3-3: use $\nabla_{\boldsymbol{P}_{g,\beta}}\varphi^{\alpha}_{\beta t_u}$ to assess the scheduled direction $\Delta\hat{\boldsymbol{P}}^{Sch_\alpha}_{g,\beta}$ from (11), which in turn is used to formulate (18). The solution of (18) obtains $\Delta\boldsymbol{P}^{\alpha}_{g,\beta,\max}$. Lastly, evaluate (17) to obtain the scheduled magnitude $\Delta P^{Sch_\alpha}_{g,\beta}$.

Step 3-4: based on $\Delta\hat{\boldsymbol{P}}^{Sch_\alpha}_{g,\beta}$, $\Delta P^{Sch_\alpha}_{g,\beta}$, and OP_β, the TSC-OPF model (19) is formulated and solved to obtain the new point $OP_{\beta+1}$.

Step 3-5: let $\beta=\beta+1$, and go to *Step 3-1*.

Step 3-6: the $O\text{-}SEQ_\alpha$ sequence ends, and point $OP_{j+(n+1)}$ corresponds to the first point $OP_{in,\alpha}$, which is inside the subset S_α. Additional results are $OP_\gamma=OP_{j+n}$, the interval $T_\gamma=[OP_\gamma, OP_{in,\alpha}]$, the scheduled direction $\Delta\hat{\boldsymbol{P}}^{Sch_\alpha}_{g,\gamma}=\Delta\hat{\boldsymbol{P}}^{Sch_\alpha}_{\boldsymbol{g},j+n}$, and the scheduled magnitude $\Delta P^{Sch_\alpha}_{g,\gamma}=\Delta P^{Sch_\alpha}_{g,j+n}$.

Step 4: perform the $U\text{-}SEQ_\alpha$ sequence in the α stage. In this case, the projection operation $OP_{\gamma+1}=P^{rU}_{C\alpha}(OP_\gamma)$ must be performed as $\gamma=s, s+1,\ldots,s+m$, as described as follows.

Step 4-1: evaluate $\Delta P^{Sch_\alpha}_{g,\gamma+1}$ according to (20), and set the direction $\Delta\hat{\boldsymbol{P}}^{Sch_\alpha}_{g,\gamma+1}$ as $\Delta\hat{\boldsymbol{P}}^{Sch_\alpha}_{g,\gamma+1}=\Delta\hat{\boldsymbol{P}}^{Sch_\alpha}_{g,\gamma}$.

Step 4-2: use $\Delta\hat{\boldsymbol{P}}^{Sch_\alpha}_{g,\gamma+1}$, $\Delta P^{Sch_\alpha}_{g,\gamma+1}$, and OP_γ to formulate and solve the TSC-OPF problem (21). The solution corresponds to the $OP_{\gamma+1}$.

Step 4-3: execute the TD-SDM analysis to test η_α at $OP_{\gamma+1}$ and to obtain the new interval $T_{\gamma+1}$, as reported in Section III-B. In addition, if η_α is not satisfied, set point OP_γ as $OP_\gamma=OP_{\gamma+1}$ and increase γ as $\gamma=\gamma+1$; otherwise, set point $OP_{in,\alpha}$ as $OP_{in,\alpha}=OP_{\gamma+1}$, whereas the point OP_γ and the index γ maintain their previous values.

Step 4-4: assess the length of the interval $T_{\gamma+1}$ as $\varepsilon=T_{\gamma+1}$. If ε is greater than a specified tolerance *Tol*, go back to *Step 4-1*. Otherwise, the $U\text{-}SEQ_\alpha$ sequence ends, and the current point $OP_{in,\alpha}$ inside the subset S_α corresponds to the point OP_α on the hull of the subset S_α.

Step 4-5: if the $U\text{-}SEQ_\alpha$ sequence ends for $\alpha=$ RAC, the point OP_α is considered as the point OP_{RAC}. In this case, α must be updated as $\alpha=$ TVC, and the stabilization process goes back to *Step 2*. If the $U\text{-}SEQ_\alpha$ sequence ends for $\alpha=$ TVC, the point OP_α is set as point OP_{TVC}. This point is the solution to the TSC-OPF problem, and thus the proposed approach ends.

The procedure first performs the RAC stage and then executes the TVC stage.

In the stage α, the $O\text{-}SEQ_\alpha$ and $U\text{-}SEQ_\alpha$ sequences are performed to obtain the point OP_α on the hull of the subset S_α. Therefore, the stage α starts at point OP_j, as given in *Step 2* and conducts the $O\text{-}SEQ_\alpha$ sequence to gradually move the point towards the transient stablity region by recursively executing projection operation $P^{rO}_{C\alpha}(\cdot)$, as indicated from *Step 3-1* to *Step 3-5*. Hence, each projection operation $P^{rO}_{C\alpha}(\cdot)$ obtains a new point closer to the hull of the S_α. When the system satisfies η_α at a given new point, as tested in *Step 3-1*, the $O\text{-}SEQ_\alpha$ sequence ends, and the new point is set as the first point $OP_{in,\alpha}$ inside the set S_α. In addition, the point $OP_{in,\alpha}$ and the last point OP_γ outside the subset S_α define the upper and lower end points of the interval T_γ that bracket point OP_α, respectively. The further results needed to perform the $U\text{-}SEQ_\alpha$ sequence are given in *Step 3-6*.

The $U\text{-}SEQ_\alpha$ sequence performs a bisection having process where the projection operation $P^{rU}_{C\alpha}(\cdot)$ is recurrently executed to assess new points inside the interval T_γ, as performed from *Step 4*-1 to *Step 4-3*. This interval is reduced throughout the process by adjusting its endpoints with those assessed points. In addition, the system stability at those points must be tested, as indicated in *Step 4-3*. The $U\text{-}SEQ_\alpha$ sequence ends when the length of the interval is lower than a specified tolerance *Tol*, as verified in *Step 4-4*. With the success of this verification, the current point inside the stability region is set as the point OP_α since it satisfies η_α and is very close to the hull of the subset S_α.

When the procedure described above is satisfied in the RAC stage, the result is the point OP_{RAC} on the hull of the subset S_{RAC}. Thus, the TVC stage must be started at *Step 2*. When the TVC stage is satisfied, the transiently stable point OP_{TVC} is known.

V. Case Studies

To numerically illustrate the effectiveness of the proposed approach in solving the TSC-OPF problem, the Western System Coordinated Council (WSCC) 3-machine 9-bus system [24] and the Mexican 46-machine 190-bus equivalent system [16] are considered in this paper. The classical generator model and constant impedance loads are considered in the TD-SDM analysis, while loads are modeled as constant power for optimization studies. However, the proposed approach is entirely general, and the model used for representing a power system component is not a constraint imposed by the proposed formulation. For the TD-SDM analysis, the integration time step is 0.01 s. η_{RAC} and η_{TVC} are set as $\delta_{\max}=120°$ and $V_{\min}=0.85$ p.u. for the transient limits of rotor angles and TVS, respectively. Lastly, the percentage λ is fixed at a value of 5% for the $O\text{-}SEQ_\alpha$ sequence, whereas the convergence tolerance for the $U\text{-}SEQ_\alpha$ sequence is set as $Tol=0.01$.

A. WSCC 3-machine 9-bus System

For WSCC 3-machine 9-bus system, the likely contingency scenario is given by a permanent three-phase-to-ground fault to ground incepted at $t=0$ s at bus 7 and cleared at $t=0.35$ s by tripping the line connecting bus 7 and bus 5. The study time period is $T=[0,1]$s. The results of the stabilization process for WSCC system are reported in Table II. A conventional OPF analysis provides the point OP_U with active power re-dispatch given in row 2, columns 4 to 6, and the total generation cost reported in row 2, column 7, of Table II. The procedure is applied as follows.

Step 1 sets $\alpha=$ RAC, which starts at the point OP_{U}, as indicated in *Step 2*. For the first projection operation $P^{rO}_{\text{CRAC}}(\cdot)$ of the *O-SEQ*$_{\text{RAC}}$ sequence performed in *Step 3-1*, the TD-SDM analysis detects that the system operating at OP_{U} does not satisfy η_{RAC} given by (1) at $t_{\text{u}}=0.48$ s. In this case, OP_{U} is outside the S_{RAC}. Projections onto hulls of the subsets S_{RAC} and S_{TVC} are shown in Fig. 5, such that δ_2 surpasses the limit $\delta_{\max}=120°$ during the transient simulation. Rotor angles at the point OP_{U} in RAC stage are shown in Fig. 6. Accordingly, the TSC-OPF model (19) is assembled and solved in *Step 3-4*, with a solution given by $OP_{\text{U+1}}$ that remains outside S_{RAC}. Based on this $OP_{\text{U+1}}$, and according to *Step 3-5*, a new projection operation $P^{rO}_{\text{CRAC}}(\cdot)$ is performed. In the third projection operation of the *O-SEQ*$_{\text{RAC}}$ sequence, the TD-SDM analysis performed in *Step 3-1* detects that the first point $OP_{\text{U+3}}$ inside the subset S_{RAC} is obtained. According to *Step 3-6*, the point is set as $OP_{in,\text{RAC}}$=$OP_{\text{U+3}}$. The active power re-dispatch of each generator and the total generation cost at opint $OP_{in,\text{RAC}}$ are given in row 3 of Table II. The *O-SEQ*$_{\text{RAC}}$ sequence ends according to *Step 3-6*.

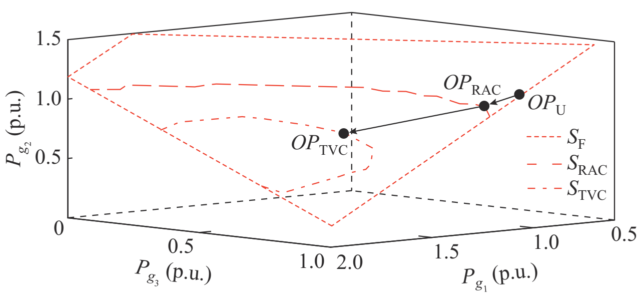

Fig. 5. Projections onto hulls of subsets of S_{RAC} and S_{TVC}.

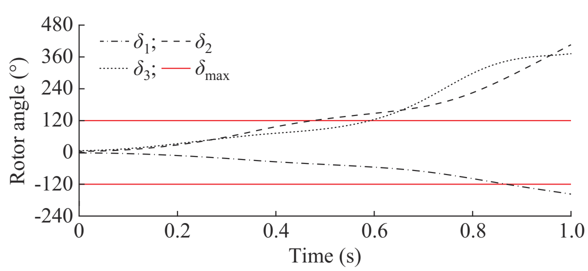

Fig. 6. Rotor angle at OP_{U}.

The *U-SEQ*$_{\text{RAC}}$ sequence is now executed by using the projection operation $P^{rU}_{\text{CRAC}}(\cdot)$ to formulate and solve the TSC-OPF model (21) in *Step 4-2*. The operating point obtained is provided to *Step 4-3*, where the TD-SDM analysis declares that the system satisfies η_{RAC}. In addition, the criterion stated in *Step 4-4* is satisfied for the specified tolerance *Tol*. Based on these results, the operating point is declared as point OP_{RAC}, thus ending both *U-SEQ*$_{\text{RAC}}$ and RAC stage. The active power re-dispatch and total generation cost for OP_{RAC} are given in row 4 of Table II. Rotor angles at OP_{RAC} are shown in Fig. 7. Figure 7 clearly shows that the limit $\delta_{\max}=120°$ is satisfied for point OP_{RAC}, which is located on the hull of the subset S_{RAC}, as shown in Fig. 5.

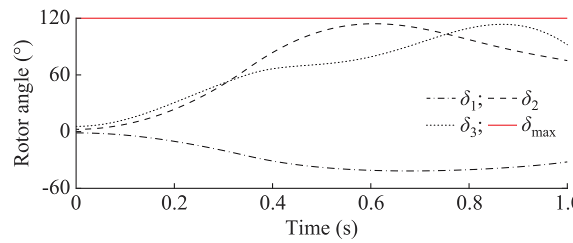

Fig. 7. Rotor angle at OP_{RAC}.

According to *Step 4-5*, point OP_{RAC} is used to start the TVC stage in *Step 2*. In *Step 3-1* of the first projection operation $P^{rO}_{\text{CTVC}}(\cdot)$ of the *O-SEQ*$_{\text{TVC}}$ sequence, the TD-SDM analysis indicates that the system operating at OP_{RAC} and subjected to the contingency scenario does not satisfy η_{TVC} given by (3) at $t_{\text{u}}=0.36$ s. In this case, there are transient trajectories of voltage magnitudes surpassing $V_{\min}=0.85$ p.u.. Transient voltages at OP_{RAC} are shown in Fig. 8. Hence, point OP_{RAC} is outside S_{TVC}, as clearly shown in Fig. 5. To achieve a transiently stable operating point, the *O-SEQ*$_{\text{TVC}}$ sequence performs a total of 10 single projection operations $P^{rO}_{\text{CTVC}}(\cdot)$ to assess the first point inside the subset S_{TVC}, which is set as $OP_{in,\text{TVC}}=OP_{\text{RAC+10}}$ in *Step 3-6*. The active power re-dispatch and the total generation cost for $OP_{\text{RAC+10}}$ are given in row 5 of Table II.

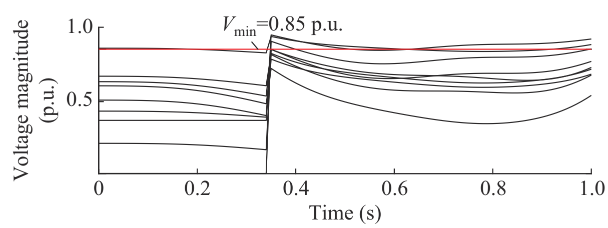

Fig. 8. Transient voltages at OP_{RAC}.

TABLE II
RESULTS OF STABILIZATION PROCESS FOR WSCC SYSTEM

α	Sequence	Point	P_{g_1} (MW)	P_{g_2} (MW)	P_{g_3} (MW)	Cost ($/hour)
	Base point	OP_{U}	105.94	113.04	99.24	1132.2
RAC	*O-SEQ*$_{\text{RAC}}$	$OP_{in,\text{RAC}}$	121.17	101.91	94.83	1134.8
	U-SEQ$_{\text{RAC}}$	OP_{RAC}	118.24	104.36	95.35	1133.9
TVC	*O-SEQ*$_{\text{TVC}}$	$OP_{in,\text{TVC}}$	160.33	82.90	74.36	1163.4
	U-SEQ$_{\text{TVC}}$	OP_{TVC}	160.12	83.05	74.41	1163.1

The *O-SEQ*$_{\mathrm{TVC}}$ sequence results reported above are transferred to the *U-SEQ*$_{\mathrm{TVC}}$ sequence, which starts in *Step 4*. In this case, three single projection operations $P^{rU}_{\mathrm{CTVC}}(\cdot)$ are performed to assess point OP_{TVC} on the hull of the subset S_{TVC}. Hence, the sequence and the proposed approach end in *Step 4-5* of the third projection operation. Rotor angle at OP_{TVC} and transient voltages at OP_{TVC}, as shown in Fig. 9 and Fig. 10, reveal that both criteria η_{RAC} and η_{RAC} are satisfied, respectively. Furthermore, the active power re-dispatch required to achieve this transiently stable operating point and its associated total generation cost are given in row 6 of Table II.

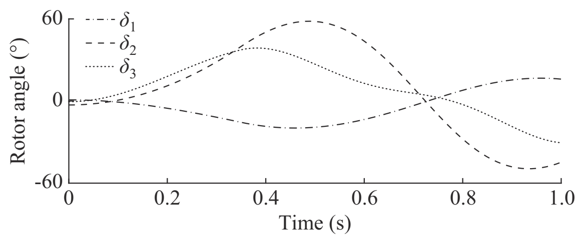

Fig. 9. Rotor angles at OP_{TVC}.

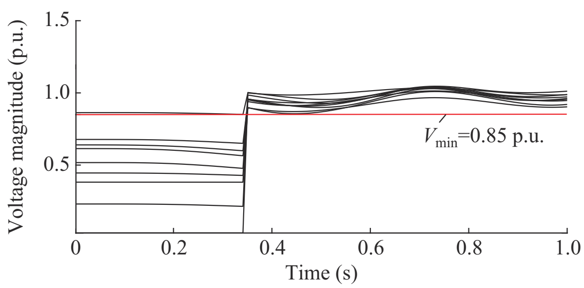

Fig. 10. Transient voltages at OP_{TVC}.

Lastly, the comparison of results with the proposed approach and the global approach [7] is shown in Table III, which compares the active power re-dispatch, total generation cost, and CPU time related to the solution to the TSC-OPF problem. Note that the active power re-dispatch and total generation cost compare well, whereas the total CPU time required by the proposal in this paper is 95.4% lower than that required by the global approach, which clearly shows the prowess of the proposed approach.

TABLE III
COMPARISON OF RESULTS WITH PROPOSED APPROACH AND GLOBAL APPROACH

Approach	P_{g_1} (MW)	P_{g_2} (MW)	P_{g_3} (MW)	Cost ($/h)	Total CPU time (s)
Global	157.94	82.57	77.27	1161.40	201.04
Proposed	160.33	82.90	74.36	1163.40	9.18

B. Mexican 46-machine 190-bus Equivalent System

The proposed approach is applied to a reduced model of the Mexican interconnected power system (MIPS) composed of 46 generators, 91 loads, and 265 transmission components, with its topological structure and nomenclature reported in [16]. The representative diagram of MIPS is summarized in Fig. 11.

For the MIPS, the contingency scenario is given by a permanent three-phase-to-ground fault incepted at bus 182 at $t=0$ s and cleared at $t=0.15$ s by tripping the line connecting buses 182 and 86. The study period is $T=[0,5]$s. A conventional OPF analysis is executed to obtain the base point OP_{U}, which results in the total generation cost given in row 2, column 4 of Table IV.

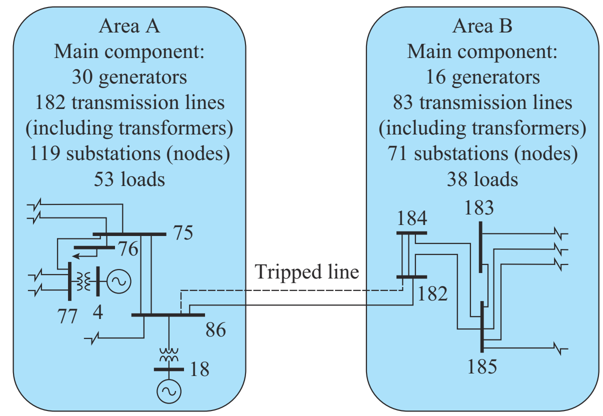

Fig. 11. Representative diagram of MIPS.

TABLE IV
COSTS OF OPS FOR MIPS

α	Sequence	Point	Cost ($/hour)
	Base point	OP_{U}	21093.4
RAC	*O-SEQ*$_{\mathrm{RAC}}$	$OP_{in,\mathrm{RAC}}$	21408.8
	U-SEQ$_{\mathrm{RAC}}$	OP_{RAC}	21106.4
TVC	*O-SEQ*$_{\mathrm{TVC}}$	$OP_{in,\mathrm{TVC}}$	21448.5
	U-SEQ$_{\mathrm{TVC}}$	OP_{TVC}	21111.0

Step 1 sets $\alpha=$RAC and point OP_{U} is used to start the *O-SEQ*$_{\mathrm{RAC}}$ sequence from *Step 2*. The TD-SDM analysis related to the first projection operation $P^{rO}_{\mathrm{CRAC}}(\cdot)$ is executed in *Step 3-1* and detects that some transient trajectories of rotor angles surpass the limit $\delta_{\max}=120°$. Rotor angles at point OP_{U} are shown in Fig. 12. The system is declared unstable at $t_{\mathrm{u}}=0.59$ s. The TSC-OPF problem is then formulated and solved in *Step 3-4* to obtain the point $OP_{\mathrm{U}+1}$, where the total generation cost is given in row 3 of Table IV. The *O-SEQ*$_{\mathrm{RAC}}$ sequence returns to *Step 3-1*, where the TD-SDM determines that η_{RAC} is satisfied. The *O-SEQ*$_{\mathrm{RAC}}$ sequence ends in *Step 3-6* with the system operating point given by $OP_{in,\mathrm{RAC}}=OP_{\mathrm{U}+1}$.

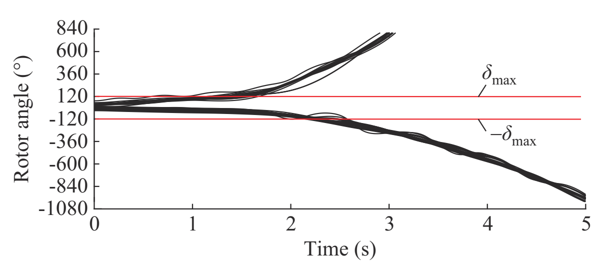

Fig. 12. Rotor angles at OP_{U}.

The projection operation $P^{rU}_{\mathrm{CRAC}}(\cdot)$ is now applied to perform the *U-SEQ*$_{\mathrm{RAC}}$ sequence in *Step 4*. After seven executions of this operation, OP_{RAC} is obtained on the hull of the subset S_{RAC} with the total operating cost given in row 4 of Table IV. The corresponding rotor angles at OP_{RAC} and transient voltages at OP_{RAC} are shown in Figs. 13 and 14, respectively. It is noted that the rotor angle limit $\delta_{\max}=120°$ is satisfied. The transient voltage limit $V_{\min}=0.85$ p.u., however, is not satisfied at $t_u=0.96$ s.

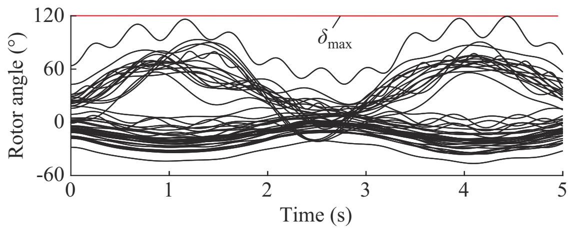

Fig. 13. Rotor angles at OP_{RAC}.

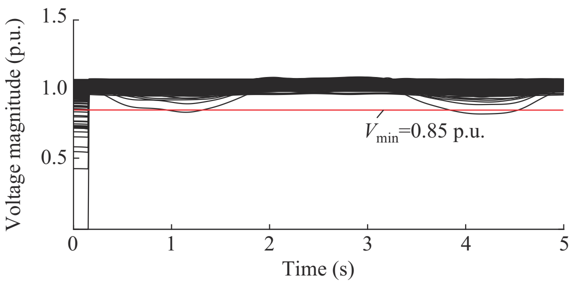

Fig. 14. Transient voltages at OP_{RAC}.

The stabilization process for voltage magnitudes is now performed through the TVC stage by considering OP_{RAC} as the starting point of this process. When $\alpha=\text{TVC}$, the $O\text{-}SEQ_{\text{TVC}}$ sequence performs one projection operation $P_{\text{CTVC}}^{rO}(\cdot)$ to obtain the point $OP_{\text{RAC}+1}$, where η_{TVC} is satisfied. This point is set as $OP_{in,\text{TVC}}=OP_{\text{RAC}+1}$ in *Step 3-6* with a generation cost given in row 5 of Table IV. Lastly, the $U\text{-}SEQ_{\text{TVC}}$ sequence is executed and seven projection operations $P_{\text{CTVC}}^{rU}(\cdot)$ are conducted to obtain point OP_{TVC}. The system operating at OP_{TVC} and subjected to the specified contingency scenario satisfies both criteria η_{RAC} and η_{TVC}, which is corroborated by the rotor angle at OP_{TVC} and transient voltages at OP_{TVC}, as shown in Figs. 15 and 16, respectively.

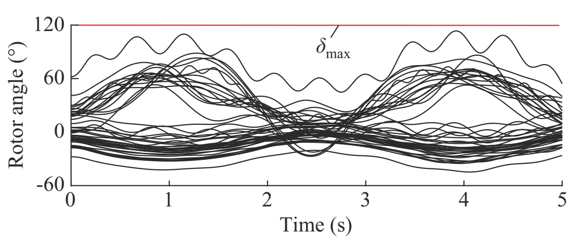

Fig. 15. Rotor angles at OP_{TVC}.

Furthermore, the corresponding generation cost of point OP_{TVC} is given in row 6 of Table IV.

Finally, the total generation costs shown in Table IV clearly reveal that the most economic generation cost corresponds to the transiently unstable point OP_{U}.

Point OP_{RAC} only ensures the rotor angle stability with a cost increase of 0.06% with regard to the cost associated with point OP_{U}. Lastly, the criteria of rotor angles and voltage magnitudes are simultaneously satisfied for the specified contingency scenario when the system is operating at point OP_{TVC}, which increases the generation cost of point OP_{U} by only 0.08%. Results show that the generation cost slightly increases with the improvement of the power system security through the proposed approach, although the total power re-dispatch for assessing point OP_{TVC} is 56.6 MW. The CPU time required to solve the TSC-OPF problem is 218.89 s.

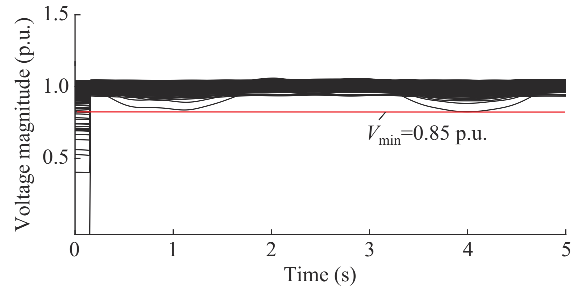

Fig. 16. Transient voltages at OP_{TVC}.

VI. Conclusion

A sequential TSC-OPF approach is proposed to accurately assess the most economical operating point that simultaneously satisfies η_{RAC} and η_{TVC} when a power system is subjected to a specified contingency scenario. In this preventive control, the evolution of the transient trajectories corresponding to rotor angles and voltage magnitudes is bounded through an economic active power re-dispatch, which is performed to guide the system to a normal operating state. For this purpose, the TSC-OPF problem is formulated as two mutually connected subproblems. The first is associated with a conventional OPF problem extended with only two additional active power re-dispatch constraints based on projections onto sets. The second relates to the transient stability assessment that determines the evolutions of rotor angles and voltage magnitudes and provides the information required to assemble the active power re-dispatch stability constraints. In this paper, the TSC-OPF model has a dimension, complexity, and computational burden similar to that of a conventional OPF model because including discretized constraints in the formulation is unnecessary.

Numerical results clearly demonstrate the effectiveness of the proposed approach in solving the TSC-OPF problem and avoiding system unstable operation. Concerning the 3-machine 9-bus system, the cost of performing the preventive control through the proposed approach and the global SD approach is 2.73% and 2.58% higher than the base cost associated with the transiently insecure base operating point, respectively. In case studies, the computational time required to achieve the preventive control is 9.18 s and 201.04 s for the proposed approach and the global SD approach, respectively. Hence, the proposed approach is only 0.1464% more expensive than that obtained by the SD approach, saving 95.4% of CPU time. The solution obtained by the proposed approach compares well with that provided by the global SD approach but with the advantage of avoiding the resolution of an optimal problem of enormous dimension, complexity and computational burden. The case study associated with the MIPS shows that the cost of generation re-dispatch for maintaining the system secure operation is only 0.08% more expensive than the corresponding transiently insecure base operating point. The proposed approach achieves the preventive control of this 46-machine 190-bus system in 218.89 s, which is very similar to the CPU time required by the global SD approach to stabilize the 3-machine 9-bus system, which is 201.04 s. This comparison of computational performances verifies the computational savings achieved by the proposed approach.

Since the proposed approach is based on the well-known projections onto set concept, two different feasible regions have been straightforwardly addressed to solve the TSC-OPF problem. Hence, a basis for handling the multi-contingency case is provided because the stability region for each contingency could be defined as a set of points for the non-heuristic solution to the multi-contingency TSC-OPF problem. This is an important topic that the authors will address in a forthcoming publication.

References

[1] T. Weckesser, H. Jóhannsson, J. Østergaard *et al*., "Derivation and application of sensitivities to assess transient voltage sags caused by rotor swings," *International Journal of Electrical Power & Energy Systems*, vol. 72, pp. 75-82, Nov. 2015.

[2] M. Pertl, T. Weckesser, M. Rezkalla *et al*., "Transient stability improvement: a review and comparison of conventional and renewable-based techniques for preventive and emergency control," *Electrical Engineering*, vol. 100, no. 3, pp. 1701-1718, Sept. 2018.

[3] S. Abhyankar, G. Geng, M. Anitescu *et al*., "Solution techniques for transient stability-constrained optimal power flow – part I," *IET Generation*, *Transmission & Distribution*, vol. 11, no. 12, pp. 3177-3185, Aug. 2017.

[4] Y. Xu, Y. Chi, and H. Yuan, *Stability-constrained Optimization for Modern Power System Operation and Planning*, 1st. New York: Wiley, 2023.

[5] M. L. Scala, M. Trovato, and C. Antonelli, "On-line dynamic preventive control: an algorithm for transient security dispatch," *IEEE Transactions on Power Systems*, vol. 13, no. 2, pp. 601-610, May 1998.

[6] D. Gan, R. Thomas, and R. Zimmerman, "Stability-constrained optimal power flow," *IEEE Transactions on Power Systems*, vol. 15, no. 2, pp. 535-540, May 2000.

[7] E. de Tuglie, M. L. Scala, and P. Scarpellini, "Real-time preventive actions for the enhancement of voltage-degraded trajectories," *IEEE Transactions on Power Systems*, vol. 14, no. 2, pp. 561-568, May 1999.

[8] F. Capitanescu, J. Ramos, P. Panciatici *et al*., "State-of-the-art, challenges, and future trends in security constrained optimal power flow," *Electric Power Systems Research*, vol. 81, no. 8, pp. 1731-1741, Aug. 2011.

[9] G. Geng, S. Abhyankar, X. Wang *et al*., "Solution techniques for transient stability-constrained optimal power flow – Part II," *IET Generation*, *Transmission & Distribution*, vol. 11, no. 12, pp. 3186-3193, Aug. 2017.

[10] Q. Jiang, Z. Huang, and K. Xu, "Contingency filtering technique for transient stability constrained optimal power flow," *IET Generation*, *Transmission & Distribution*, vol. 7, no. 12, pp. 1536-1546, Dec. 2013.

[11] G. Geng, V. Ajjarapu, and Q. Jiang, "A hybrid dynamic optimization approach for stability constrained optimal power flow," *IEEE Transactions on Power Systems*, vol. 29, no. 5, pp. 2138-2149, Sept. 2014.

[12] Y. Sun, Y. Xin, and H. Wang, "Approach for optimal power flow with transient stability constraints," *IEE Proceedings: Generation*, *Transmission and Distribution*, vol. 151, no. 1, p. 8, Jan. 2004.

[13] D. Ruiz-Vega and M. Pavella, "A comprehensive approach to transient stability control: part I – near optimal preventive control," *IEEE Transactions on Power Systems*, vol. 18, no. 4, pp. 1446-1453, Nov. 2003.

[14] T. B. Nguyen and M. A. Pai, "Dynamic security-constrained rescheduling of power systems using trajectory sensitivities," *IEEE Transactions on Power Systems*, vol. 18, no. 2, pp. 848-854, May 2003.

[15] A. Pizano-Martinez, C. R. Fuerte-Esquivel, and D. Ruiz-Vega, "A new practical approach to transient stability-constrained optimal power flow," *IEEE Transactions on Power Systems*, vol. 26, no. 3, pp. 1686-1696, Aug. 2011.

[16] A. Pizano-Martínez, C. R. Fuerte-Esquivel, E. Zamora-Cárdenas *et al*., "Selective transient stability-constrained optimal power flow using a SIME and trajectory sensitivity unified analysis," *Electric Power Systems Research*, vol. 109, pp. 32-44, Apr. 2014.

[17] L. Tang and W. Sun, "An automated transient stability constrained optimal power flow based on trajectory sensitivity analysis," *IEEE Transactions on Power Systems*, vol. 32, no. 1, pp. 590-599, Jan. 2017.

[18] Y. Xu, J. Ma, Z. Dong *et al*., "Robust transient stability-constrained optimal power flow with uncertain dynamic loads," *IEEE Transactions on Smart Grid*, vol. 8, no. 4, pp. 1911-1921, Jul. 2017.

[19] A. Pizano-Martinez, C. Fuerte-Esquivel, E. A. Zamora-Cardenas *et al*., "Directional derivative-based transient stability-constrained optimal power flow," *IEEE Transactions on Power Systems*, vol. 32, no. 5, pp. 3415-3426, Sept. 2017.

[20] H. Yuan and Y. Xu, "Trajectory sensitivity based preventive transient stability control of power systems against wind power variation," *International Journal of Electrical Power & Energy Systems*, vol. 117, p. 105713, May 2020.

[21] S. Xia, Z. Ding, M. Shahidehpour *et al*., "Transient stability-constrained optimal power flow calculation with extremely unstable conditions using energy sensitivity method," *IEEE Transactions on Power Systems*, vol. 36, no. 1, pp. 355-365, Jan. 2021.

[22] A. Zilinskas, "Feasibility and infeasibility in optimization: algorithms and computational methods," *Interfaces*, vol. 39, no. 3, pp. 292-295, Oct. 2009.

[23] P. L. Combettes, "The convex feasibility problem in image recovery," *Advances in Imaging and Electron Physics*, vol. 95, pp. 155-270, Jan. 1996.

[24] A. Pizano-Martínez, E. Z. Cárdenas, C. Fuerte-Esquivel *et al*., "Unified analysis of single machine equivalent and trajectory sensitivity to formulate a novel transient stability-constrained optimal power flow approach," *Electric Power Components and Systems*, vol. 42, no. 13, pp. 1386-1397, Oct. 2014.

[25] A. Zamora-Cárdenas and C. Fuerte-Esquivel, "Multi-parameter trajectory sensitivity approach for location of series-connected controllers to enhance power system transient stability," *Electric Power Systems Research*, vol. 80, no. 9, pp. 1096-1103, Sept. 2010.

Jorge Uriel Sevilla-Romero received the B.E. degree from Instituto Tecnológico de Orizaba, Orizaba, México, in 2009, and the M.S. degree from the Instituto Politécnico Nacional, México City, México, in 2013. He is currently pursuing the Ph.D. degree in the electrical engineering graduate program of the Universidad Michoacana de San Nicolás de Hidalgo, Morelia, México. His research interest includes optimal operation, dynamic and steady-state analysis of electric power system.

Claudio Rubén Fuerte-Esquivel received his B.E. degree (Hons.) from Instituto Tecnológico de Morelia, Morelia, México, in 1990, the M.S. degree (summa cum laude) from Instituto Politécnico Nacional, México City, México, in 1993, and the Ph. D. degree from the University of Glasgow, Scotland, UK, in 1997. Currently, he is a Full-time Professor at Universidad Michoacana de San Nicolás de Hidalgo, Morelia, México. His research interest includes dynamic-state and steady-state analysis of flexible AC transmission system.

Alejandro Pizano-Martínez received the B.E. degree (Hons.) from Universidad de Colima, Colima, Mexico, in 2001, and the M.S. and Ph.D. degrees from the electrical engineering graduate program of the Universidad Michoacana, Morelia, México, in 2004 and 2010, respectively. Currently, he is a Full-time Professor at Universidad of Guanajuato, Salamanca, México. His research interest includes optimal operation, dynamic-state and steady-state analysis of electric power system.

Reymundo Ramírez-Betancour received the B.E. degree (Hons.) from Instituto Tecnológico de Lázaro Cárdenas, Lázaro Cárdenas, México, in 2001, and the M.S. and Ph.D. degrees from the electrical engineering graduate program of the Universidad Michoacana, Morelia, México, in 2006 and 2012, respectively. Currently, he is a Full-time Professor at Universidad Juárez Autónoma de Tabasco, Villahermosa, México. His research interest includes optimal operation, dynamic-state and steady-state analysis of electric power system.